Molecular and Cellular Biochemistry
https://doi.org/10.1007/s11010-024-04956-8

Abnormal upregulation of NUBP2 contributes to cancer progression in colorectal cancer

Danfeng Lan[1] · Junyu Wang[2] · Guishun Sun[2] · Lixia Jiang[2] · Qiyun Chen[2] · Sha Li[2] · Haiyan Qu[2] · Yibo Wang[2] · Bian Wu[2]

Received: 21 August 2023 / Accepted: 3 February 2024

Abstract

Colorectal cancer (CRC), a digestive tract malignancy with high mortality and morbidity, lacks effective biomarkers for clinical prognosis due to its complex molecular pathogenesis. Nucleotide binding protein 2 (NUBP2) plays a vital role in the assembly of cytosolic Fe/S protein and has been implicated in cancer progression. In this study, we found that NUBP2 was highly expressed in CRC by TCGA database analysis. Subsequently, we verified the expression of NUBP2 in CRC tumor tissues and para-carcinoma tissues using IHC staining, and further investigated its association with clinicopathological parameters. In vitro cell experiments were conducted to assess the role of NUBP2 in CRC by evaluating cell proliferation, migration, and apoptosis upon NUBP2 dysregulation. Furthermore, we established a subcutaneous CRC model to evaluate the impact of NUBP2 on tumor growth in vivo. Additionally, we performed mechanistic exploration using a Human Phospho-Kinase Array-Membrane. Our results showed higher expression of NUBP2 in CRC tissues, which positively correlated with the pathological stage, indicating its involvement in tumor malignancy. Functional studies demonstrated that NUBP2 knockdown reduced cell proliferation, increased apoptosis, and impaired migration ability. Moreover, NUBP2 knockdown inhibited tumor growth in mice. We also observed significant changes in the phosphorylation level of GSK3β upon NUBP2 knockdown or overexpression. Additionally, treatment with CHIR-99021 HCl, an inhibitor of GSK3β, reversed the malignant phenotype induced by NUBP2 overexpression. Overall, this study elucidated the functional role of NUBP2 in CRC progression both in vitro and in vivo, providing insights into the molecular mechanisms underlying CRC and potential implications for targeted therapeutic strategies.

Keywords Colorectal cancer · NUBP2 · GSK3β · Malignant phenotype · Tumor growth

Introduction

Colorectal cancer (CRC) is a common digestive tract malignancy contains colon and rectal cancer [1]. According to statistics, in 2020, there are approximately 1.93 million new cases, 916 000 deaths from CRC in the world annually (https://www.who.int/news-room/fact-sheets/detail/cancer), imposing a huge economic burden on the whole society.

Surgery is the standard treatment for early stage CRC [2]. Whereas most patients are diagnosed with CRC at an advanced stage, by which metastasis has occurred and eventually succumb to the disease [3]. As therapeutic technology, including surgery combined with chemotherapy or radiotherapy has progressed, many breakthroughs have been made in the treatment of CRC [4]. Regrettably, tumor recurrence, distant metastasis, drug resistance and toxic effects are still a worldwide difficult for the clinician. Over the past

Danfeng Lan and Junyu Wang contributed equally as co-first authors.

✉ Bian Wu
13987172118@163.com

[1] Department of Gastroenterology, The First People's Hospital of Yunnan Province, The Affiliated Hospital of Kunming University of Science and Technology, Kunming 650032, Yunnan, China

[2] Department of General Surgery II, The First People's Hospital of Yunnan Province, The Affiliated Hospital of Kunming University of Science and Technology, No. 157, Jingbi Road, Kunming 650032, Yunnan, China

Published online: 16 March 2024

dozen years, many molecules associated with cancer have been identified, and targeting these biomarkers are essential for the development of targeted therapy in metastatic CRC [5–7]. However, the clinical outcomes were not approving enough, and the effective biomarkers for the clinical prognosis of CRC remain to be widely investigated due to its heterogeneous and intricate molecular pathogenesis.

Nucleotide binding protein 2 (NUBP2), located in the t-complex region of mouse Chromosome 17, is a conserved and vital protein in Eukaryotes [8]. NUBP1 and NUBP2 play a crucial role in the cell cycle as integral components of centrioles and are involved in controlling centrosome duplication in mammalian cells [8, 9]. Moreover, NUBP2 is a key component of the cytosolic iron–sulfur (Fe/S) protein assembly, which is essential for the fundamental metabolism of all organisms [10]. A previous study demonstrated that NUBP2 is necessary for embryogenesis [11]. In Barrett's esophagus with high-grade dysplasia, suppressing NUBP2 significantly impacts cell morphology [12]. Furthermore, RNA-sequencing analysis identified it as a potential biomarker for diagnosing sarcopenia [13]. Aberrant NUBP2 expression has also been observed in several cancers, including gastric cancer [14] and hepatocellular carcinoma [15]. However, the functional role of NUBP2 in CRC remains unclear.

In the current study, the expression patterns of NUBP2 in the CRC tissues and cell lines were firstly compared with the normal tissues and cells. Subsequently, in vitro functional assays were performed to verify the biological role of NUBP2 in the regulation of CRC cell malignant behaviors through NUBP2 knockdown. Additionally, the effects of NUBP2 knockdown on the tumor growth in vivo were investigated in a CRC xenograft model. These findings provided evidence supporting the potential of NUBP2 as a target for the development of novel therapeutic interventions against CRC.

Materials and methods

Cell lines, tissue microarray, and animals

Human CRC cell lines RKO, HT29 and HCT 116, as well as human normal colonic epithelial cells FHC, were obtained from ATCC and cultured in 1640 medium supplemented with 10% fetal bovine serum (FBS). All cell lines were kept in a 37 °C incubator with 5% CO_2.

A tissue microarray generated from 114 CRC tissues and 94 normal para-carcinoma tissues was provided by Shanghai Yibeirui Biomedical Science and Technology Co., Ltd. (Shanghai, China). The patients' clinical baseline data were collected with their written informed consent.

Four-week-old female BALB/c nude mice were obtained from Gempharmatech Co., Ltd. in Jiangsu, China. The mice were housed in groups of five per cage under controlled conditions, including a temperature of 22–25 °C, humidity of 50–60%, and a 12-h light/dark cycle. Ample food and water were provided to the mice.

Immunohistochemistry (IHC) staining

Section samples were dewaxed in xylene and then rehydrated through graded ethanol (100%, 95%, 85% and 75%). The sections were washed in flowing water and subjected to antigen retrieval with using citrate buffer (pH 6.0) before blocking endogenous peroxidase activity with 3% H_2O_2 for 5 min. Subsequently, the sections were blocked with 5% normal serum and incubated with primary antibodies (NUBP2, 1:100, Sanying, #15409-1-AP; Ki-67, 1:100, Abcam, #ab16667) overnight at 4 °C. After washing, secondary antibody (goat anti-rabbit IgG H& L (HRP): 1:400, Abcam, #ab97080) was added for incubation of sections. Afterwards, DAB coloration and hematoxylin counterstaining were performed (Baso Diagnostics Inc., Zhuhai, China). The slides were sealed with neutral resin, and images were captured under microscope. The scoring system takes into account both the level and the amount of staining. The IHC scoring method was used to evaluate the images, using a scale that ranges from negative (0), positive (1–4), ++ positive (5–8), to +++ positive (9–12), as has been previously described [16].

Establishment of stably infected cells

Three different short hairpin (shNUBP2-1: 5′-GATGGGAATCGTGGAGAATAT-3′, shNUBP2-2: 5′-GCGAGCTGACCTTCTGTAGGA-3′, and shNUBP2-3: 5′-GCCACCATAGAAGCCCTGCGT-3′) were used to specifically targeting NUBP2 gene. A randomly rearranged sequence, 5′-TTCTCCGAACGTGTCACGT-3′, was utilized as a negative control for shRNA (shCtrl). After annealing, the double-stranded DNA oligos were joined with a linearized vector through T4 DNA ligase. The resulting recombinant vector was then transformed into competent Escherichia coli cells and cultured in LB medium supplemented with ampicillin at 37 °C. The plasmid was extracted using the EndoFree Maxi Plasmid Kit (TIANGEN, China) following the manufacturer's instructions. For lentivirus production, plasmids, pMD2.G (Qiagen, China), and psPAX2 (Qiagen, China) were transfected into 293T cells using Lipofectamine® 2000 (Thermo Fisher, USA).

Seeding cells in 6-well plates at a density of 5×10^4 cells per well and incubating them at 37 °C with 5% CO_2. The lentivirus vector or control virus was added to the culture when the cells reached 30–50% confluency and incubated

for 24 h. Subsequently, puromycin (2 μg/mL) was introduced to the medium to select and maintain the infected cells for further experiments.

Quantitative real-time PCR (qRT-PCR)

The cells were used to isolate Total RNA, by following the manufacturer's protocol, with the TRIzol® reagent (Sigma, USA). The purity and concentration of the RNA extracted were evaluated by Nanodrop 2000/2000C spectrophotometry (Thermo, USA). Next, the cDNA was synthesized using the Hiscript QRT supermix according to the manufacturer's instructions (Vazyme, China). qRT-PCR performed using SYBR Green mastermix (Vazyme, China). For normalization purposes, GAPDH was utilized as an internal control. The $2^{-\Delta\Delta Ct}$ method was employed to determine the relative expression levels. The primers sequences (5′–3′) were listed as follows: the forward primer of NUBP2 is GTGGAGAGG CCCCAAGAAAA, the reverse primer is TAGGGACGC AGGGCTTCTAT; the forward primer of GAPDH is TGA CTTCAACAGCGACACCCA, the reverse primer is CAC CCTGTTGCTGTAGCCAAA.

Western blot analysis

The cells were lysed with lysis buffer on ice for a period of 30 min. The concentration of proteins was determined using the BCA protein assay kit (HyClone-Pierce, USA). Later, the proteins were separated using 10% SDS-PAGE and transferred to PVDF membranes. Subsequently, the membranes were blocked with fat-free milk (5%) at room temperature for 1 h, and then exposed to primary antibodies overnight at 4 °C. The next day, the PVDF membranes were treated with secondary antibodies at room temperature for 1 h. After being washed with PBS three times, the protein bands were detected using the immobilon Western Chemiluminescent HRP Substrate kit (Millipore, USA). The antibodies used in Western blot analysis are shown in Table S1.

Celigo cell counting assay

For the Celigo cell counting assay, HCT 116 and RKO cells infected with shCtrl and shNUBP2 were seeded in 96-well plates with a density of 2×10^3 cells per well and incubated at 37 °C with 5% CO_2. The Celigo system (Nexcelom) was employed to determine the cell number for 5 consecutive days. The data obtained was subjected to statistical analysis to generate a 5-day cell growth curve.

Colony formation assay

In the colony formation assay, 2000 cells/well were seeded in a 6-well dish after being transfected for 48 h, and then cultured for 8 days until visible colonies formed. Afterwards, the cells were fixed in 4% paraformaldehyde, stained with crystal violet at room temperature for 30 min, and then the cell colonies were counted microscopically. Any shaking or moving with plates was avoided to obtain clear colonies. All experiments were performed in triplicate and repeated three times.

Flow cytometry

HCT 116 and RKO cells infected with lentivirus were cultured in 6-well plates at 37 °C. When the cells reached 85% confluence, the cells were harvested and washed with 4 °C D-Hanks solution (pH 7.2–7.4) after centrifugation at 1300 rpm. Subsequently, the cells were suspended in 200 μL of 1× binding buffer and stained with 10 μL of Annexin V-APC (#88-8007, eBioscience, China) in the absence of light for 15 min, followed by the addition of 5 μL propidium iodide (PI) solution. Cell apoptosis was assessed using the Guava easyCyte HT flow cytometer (Millipore, USA).

CCK8 assay

HCT 116 and RKO cell lines were digested, resuspended, and counted in the absence or presence of CHIR-99021 HCl (CHIR, 10 μM, SF2703-25 mg), a GSK3 inhibitor. 100 μL cell suspension was added to each well of a 96-well plate at a density of 3000 cells per well, followed by incubation for 24 h. Starting from the second day, CCK-8 reagent (10 μL) was added to each well 4 h before the end of the incubation period. After that, the 96-well plate was shaken for 2–5 min on a shaker, and the optical density (OD) was measured using a microplate reader at 450 nm for 5 consecutive days. The experiment was repeated three times.

Transwell assay

Transwell migration assays were performed to assess migration and invasion of HCT 116 and RKO cells using Transwell plates according to the the manufacturers instructions (Corning). For the cell invasion assay, the upper chamber was coated with Matrigel, whereas non-coated chamber was used for the cell migration assay. The cells in logarithmic growth period were cultured under starvation condition for 12 h and then digested by trypsin, washed by PBS for 1–2 times, resuspended in serum-free medium. Cells suspended in serum-free medium (1×10^5 cells) were seeded to the top chamber after 600 μL RPMI-1640 medium with 10% FBS was added to bottom chamber. After 12 h, non-migrated cells were removed using a cotton swab, while the migrated cells adhering to the lower surface of the membrane were fixed and stained with crystal violet at 25 °C for 3 min. Following washing with PBS, cells were imaged

using a 400× microscope in three random fields and quantified using ImageJ software (National Institutes of Health, version 1.8.0).

Mouse xenograft tumor assay

In order to establish xenograft models, BALB/c nude mice were subcutaneously injected in the right flank with RKO cells infected with shNUBP2 or shCtrl lentivirus (at a density of 1×10^7 cells/mice). The mice were then divided into shNUBP2 and shCtrl groups, respectively ($n = 6$). The size of the tumors was measured to calculate the tumor volume using the formula (tumor volume $= \pi/6 \times L \times W \times W$). After 22 days of injection, the mice were sacrificed, and the tumors were excised, weighed, and analyzed for further analysis.

Statistical analysis

Data analysis was performed using GraphPad Prism 7. The data was presented as mean ± standard deviation (SD). Analysis of variance (ANOVA) or the unpaired *t* test for two-group comparisons was used for statistical analysis. The experiments were conducted in triplicate and repeated at least three times. The Mann Whitney *U* test and Spearman's rank correlation analysis were applied to investigate the correlation between the expression of NUBP2 and tumor characteristics in patients with CRC. A *P* value lower than 0.05 was deemed statistically significant.

Results

Upregulation of NUBP2 in CRC tissues and cells

To characterize the expression of NUBP2 in CRC, we firstly analyzed the RNA sequencing (RNA-seq) data of CRC tissues from TCGA. It was found that NUBP2 expression was elevated in CRC tissues compared to normal tissues (Fig. 1A, B). Subsequently, we performed histopathological examinations using hematoxylin and eosin (HE) and IHC staining on a tissue microarray containing CRC tumor tissues and para-carcinoma tissues. HE staining was employed to assess the pathological features of CRC tissues, revealing irregular nuclear morphology, intense chromatin staining, and heterogeneous cytoplasm, whereas para-carcinoma tissues exhibited normal nuclear morphology, uniform staining (Fig. 1C). Consistently, IHC staining of NUBP2 validated the strong positive expression of NUBP2 was in CRC tissues, with particularly enhanced expression observed in tissues from stage 4 (Fig. 1D, E). Statistical analysis demonstrated that 55/114 (48.2%) of CRC tissues exhibited high NUBP2 expression, while only 1/94 (1.1%) in paracancerous tissues ($P < 0.001$) (Table 1). By analyzing the clinicopathological data, it was revealed that the expression of NUBP2 was related to metastasis and tumor stage ($P < 0.05$ for both) (Tables 2, 3). Additionally, we further verified the expression level of NUBP2 at the cellular level by RT-qPCR. As shown in Fig. 1F, the expression levels of NUBP2 in human CRC cell lines RKO, HT29 and HCT 116 were higher than the human normal colonic epithelial cells FHC. Collectively, these results implied that NUBP2 has an important role in CRC progression.

NUBP2 was successfully knocked down in CRC cells

To thoroughly survey the roles of NUBP2 in CRC, NUBP2 knockdown cell models were constructed in CRC cells by transfecting shNUBP2 or shCtrl lentiviral vector. It was found that the mRNA level of NUBP2 expression in HCT 116 cells was dramatically reduced in shNUBP2 groups compared to the shCtrl group, and shNUBP2-1 with higher knockdown efficiency (97.8%) was selected for use in the subsequent experiments (Fig. 2A). The fluorescence microscopic results indicated that HCT 116 and RKO cells were successfully infected by the lentivirus (Fig. 2B). Subsequently, we detected the knockdown efficiency of NUBP2 in HCT 116 and RKO cells by RT-qPCR and western blot assays. When compared with the shCtrl group, the expression of NUBP2 was decreased in shNUBP2 group at both mRNA and protein levels (Fig. 2C–E). Overall, these results indicated that NUBP2 was successfully knocked down in two shNUBP2 transfected CRC cell lines.

Loss of NUBP2 expression suppressed the malignant behaviors of CRC cells

Next, the effects of NUBP2 on proliferation, clone formation, apoptosis, and migration were evaluated in CRC cells upon NUBP2 silencing. Celigo cell counting assay indicated that the proliferation rates of HCT 116 and RKO cell lines were slower in shNUBP2 group than the shCtrl group ($P < 0.001$ for both) (Fig. 3A). Similarly, the colony formation efficiency was apparently weakened in HCT 116 and RKO cell lines upon NUBP2 depletion ($P < 0.01$, $P < 0.001$) (Fig. 3B). The results of flow cytometry revealed that NUBP2 knockdown significantly accelerated the apoptosis rates of HCT 116 and RKO cells compared to the shCtrl group ($P < 0.001$ for both) (Fig. 3C). Furthermore, transwell assay showed that the migration rates of HCT 116 and RKO cells in shNUBP2 group were decreased by 50% and 87%, respectively ($P < 0.001$ for both) (Fig. 3D), suggesting that NUBP2 deletion potently impaired the migratory capacity of CRC cells. Consistently, invasion of both CRC cell lines were also decreased under NUBP2 knockdown by the Transwell assay (Fig. 3E). Altogether, these results provided

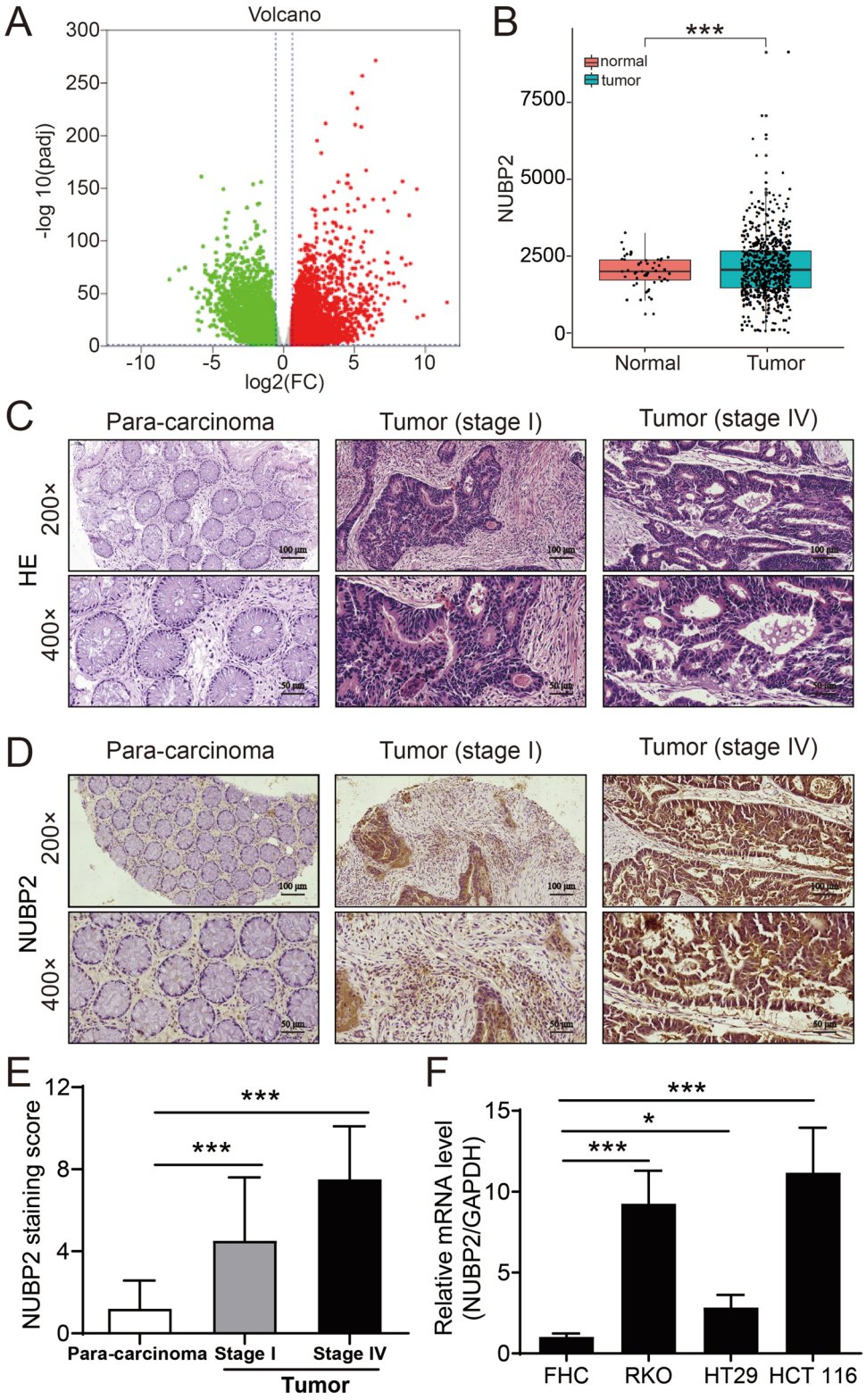

Fig. 1 NUBP2 was highly expressed in CRC tissues and cells. **A** Volcano plot for differential gene expression. **B** Comparison of NUBP2 expression levels in CRC tissues and normal tissues using TCGA RNA-seq data. **C** HE stain performed on the tissue microarray. **D** IHC staining results for the positivity of NUBP2. **E** Quantification of IHC staining results. **F** Assessment of NUBP2 mRNA expression in CRC cell lines (RKO, HT29 and HCT116) compared to the normal colon epithelial cells FHC. Results are presented as means ± SD. $*P < 0.05$ and $***P < 0.001$

evidence for the role of NUBP2 in regulating the proliferation, apoptosis, migration and invasion of CRC cells.

Moreover, the expression levels of pro-apoptotic proteins Bax and Bad were increased in shNUBP2 cells compared to the shCtrl cells (Fig. 3F). Additionally, Western blot analysis demonstrated downregulation of epithelial-mesenchymal transition (EMT) biomarkers N-Cadherin and Vimentin, while upregulation of E-cadherin upon NUBP2 knockdown

Table 1 Expression patterns in colorectal cancer tissues and para-carcinoma tissues revealed in immunohistochemistry analysis

NUBP2 expression	Tumor tissue		Para-carcinoma tissue		*P* value
	Cases	%	Cases	%	
Low	59	51.8	93	98.9	< 0.001
High	55	48.2	1	1.1	

Table 2 Relationship between NUBP2 expression and tumor characteristics in patients with colorectal cancer

Features	No. of patients	NUBP2 expression		*P* value
		Low	High	
All patients	114	59	55	
Age (years)				0.995
< 58	56	29	27	
≥ 58	58	30	28	
Gender				0.157
Male	69	32	37	
Female	45	27	18	
Tumor size				0.714
≤ 4.7 cm	58	31	27	
> 4.7 cm	56	28	28	
Stage				0.027
0	2	2	0	
I	4	3	1	
II	63	35	28	
III	40	19	21	
IV	5	0	5	
Lymphatic metastasis (N)				0.350
N0	73	40	33	
N1	31	15	16	
N2	10	4	6	
Lymph node positive (individual)				0.816
= 0	82	43	39	
> 0	32	16	16	
Metastasis				0.018
M0	109	59	50	
M1	5	0	5	

(Fig. 3F). These results further validated that NUBP2 silencing suppressed the malignant behaviors of CRC cells in vitro.

Downregulation of NUBP2 suppressed tumor growth in CRC mice

To validate the suppressive effect of NUBP2 knockdown on CRC tumor growth in vivo, a mouse xenograft model

Table 3 Relationship between NUBP2 expression and tumor characteristics in patients with colorectal cancer

		NUBP2
Metastasis	Spearman correlation	0.222
	Significance (two-tailed)	0.018
	N	114
Stage	Spearman correlation	0.208
	Significance (two-tailed)	0.027
	N	114

was established using RKO cells with or without NUBP2 knockdown. The tumor growth curves revealed that NUBP2 knockdown significantly retarded the growth of CRC tumors in mice compared to the mice of shCtrl group (Fig. 4A). After 30 days, all mice were sacrificed, and tumors were excised. It was found that the tumors formed in the shNUBP2 group of mice were smaller than those in the shCtrl group (Fig. 4B). Consistently, the tumor weight of the CRC mice in shNUBP2 group was significantly lower than that of the shCtrl group (Fig. 4C). HE staining showed a higher incidence of necrotic areas with cell body breakdown in the shCtrl group, while the shNUBP2 group exhibited organized cells and typical cellular structure (Fig. 4D). Besides, the expression of NUBP2 protein in the tissues from shNUBP2 mice was substantially downregulated compared to those in the tissues of shCtrl mice (Fig. 4E, F). These results indicated that effectively downregulating NUBP2 resulted in the suppression of tumor growth in CRC mice. In order to assess the biological significance of NUBP2 on tumor cell proliferation, IHC staining for Ki-67 (an indicator of proliferation) were performed in tumor tissues of each group. It could observe that positive expression of Ki-67 in the tissues from shNUBP2 mice was significantly weaker than the shCtrl mice tumors (Fig. 4G). Collectively, these data strongly demonstrated that downregulation of NUBP2 repressed CRC tumor progress in vivo.

NUBP2 exert critical roles in CRC progression via regulation of GSK-3β

In order to elucidate the underlying molecular mechanisms of NUBP2 in CRC progression, a human phospho-kinase array was performed in RKO cells upon NUBP2 knockdown, which could identify the essential pathway kinases that were influenced. It was observed that NUBP2 knockdown reduced the phosphorylation levels of CREB (S133), eNOS (S1177), ERK1/2 (T202/Y204, T185/Y187), Fgr (Y412), GSK-3α/β (S21/S9), GSK-3β (S9), Hsp27 (S78/S82), p53 (S15), JNK1/2/3 (T183/Y185, T221/Y223), Lyn (Y397), Msk1/2 (S376/S360), p70 S6K (T389), PLC-γ1 (Y783), RSK1/2 (S221/S227), STAT2 (Y689), STAT5a/b

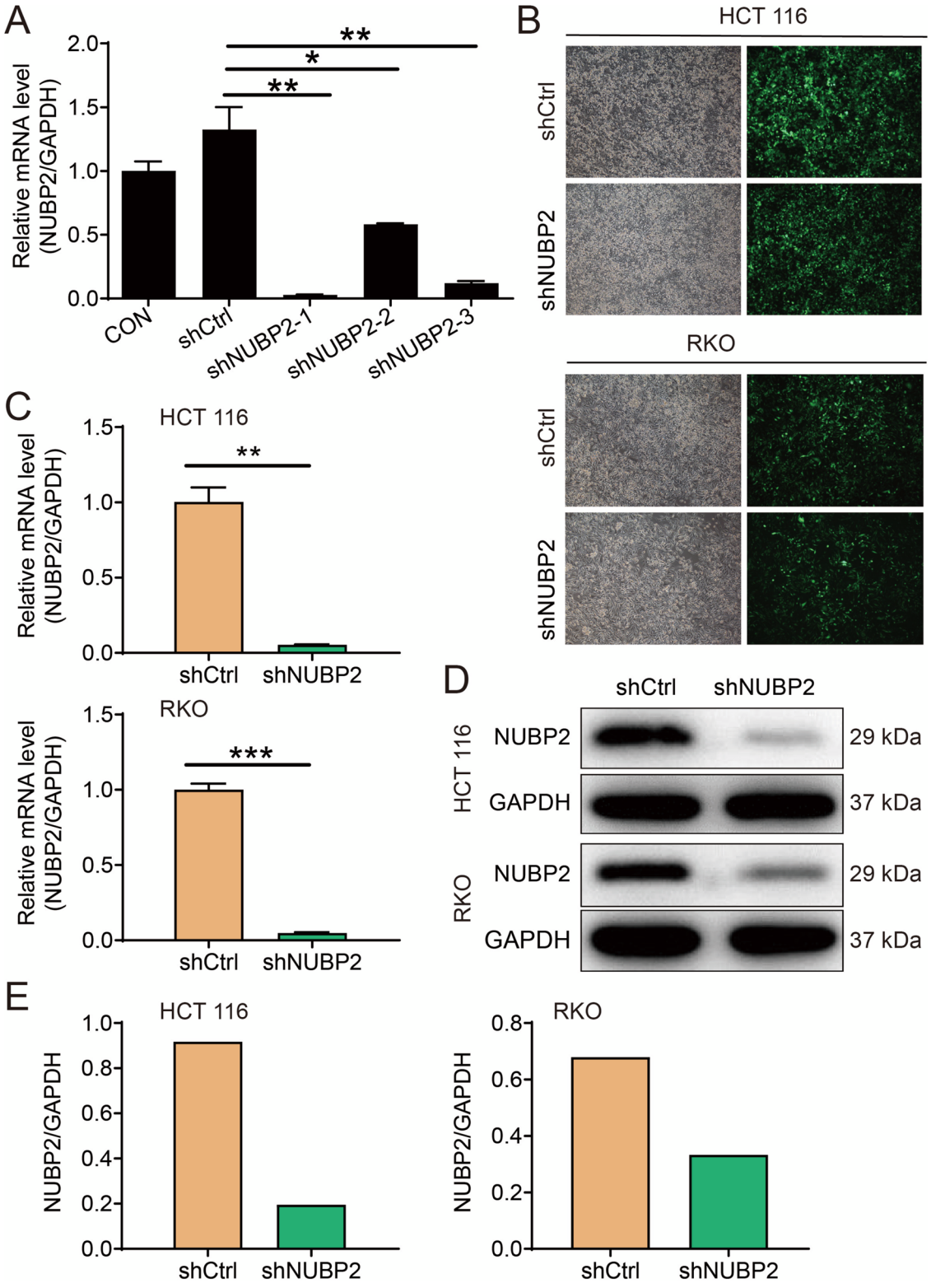

Fig. 2 Construction of NUBP2 knockdown cell models in CRC cells. **A** Three short hairpin RNA (shRNA) sequences were screened by RT-PCR. **B** Successful infection of cells was confirmed by the presence of green fluorescent protein (GFP) fluorescence. **C, D** Knockdown efficiency of NUBP2 in HCT 116 and RKO cells was assessed using RT-qPCR (**C**) and western blot (**D**) assays. **E** Quantification data of protein bands. Results are presented as means ± SD. $^{*}P < 0.05$; $^{**}P < 0.01$ and $^{***}P < 0.001$

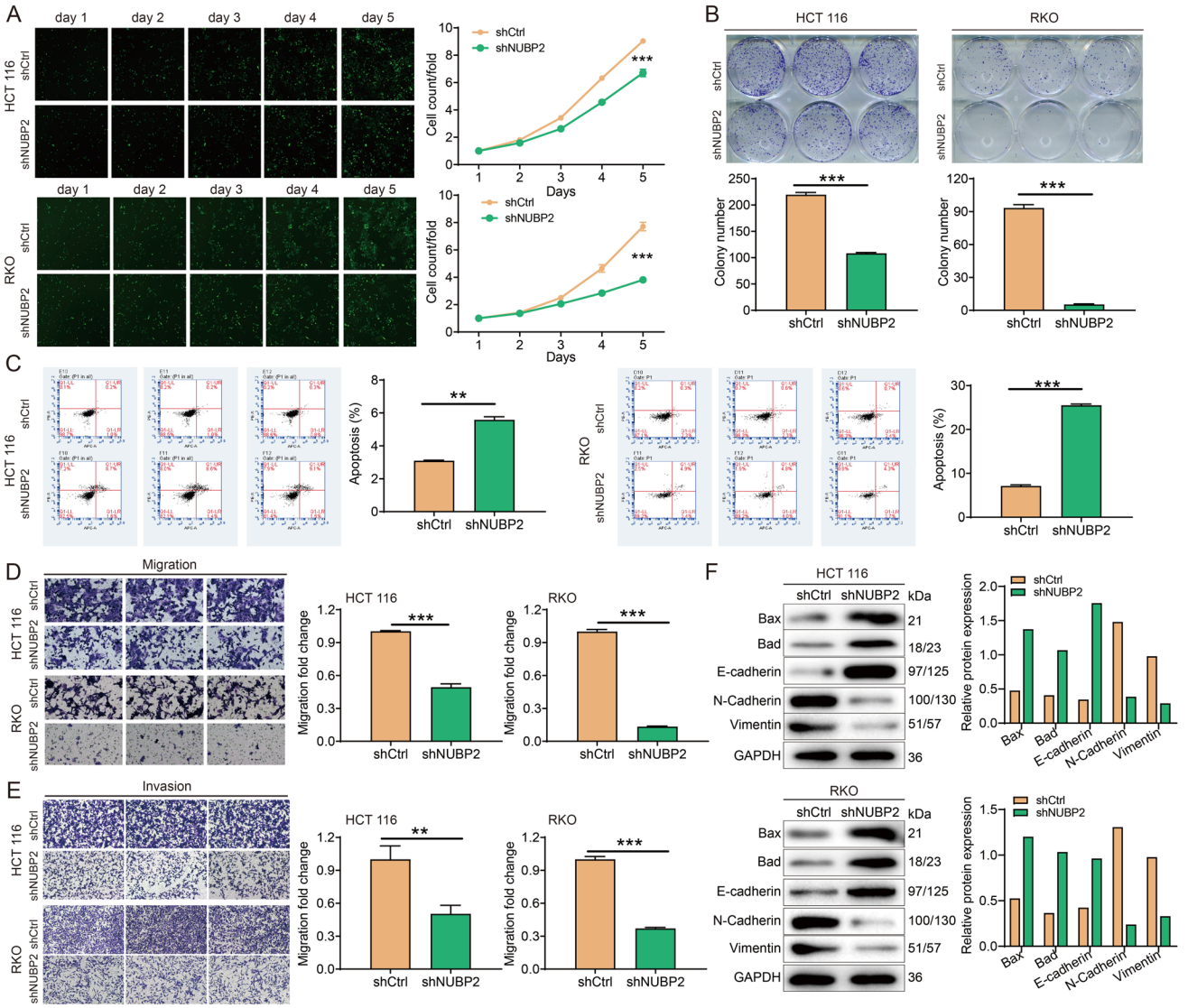

Fig. 3 NUBP2 regulated the malignant behavior of CRC cells. **A** Cell proliferation in HCT116 and RKO cell lines was evaluated using Celigo cell counting assay upon NUBP2 knockdown, and photomicrographs were captured at a ×100 magnification. **B** The cloning abilities of HCT116 and RKO cells with or without NUBP2 deletion were detected using clone formation assay. **C** Apoptosis rates of HCT116 and RKO cells were examined by flow cytometry following NUBP2 knockdown. D-E, Transwell assays were employed to measure the effect of NUBP2 knockdown on cell migration ability (**D**) and invasion ability (**E**) of both CRC cell lines. Representative images were captured at magnifications of ×200 for migration and ×100 for invasion, respectively. F, Western blot analysis was performed to assess the apoptotic markers and EMT markers after NUBP2 knockdown. Results are presented as means ± SD. $^{**}P < 0.01$ and $^{***}P < 0.001$

(Y694/Y699) and WNK1 (T60) compared to the shCtrl group (Fig. 5A). Next, we focused on GSK-3 in the following study, as it underwent the most significant down-regulation. The GSK3 inhibitor CHIR-99021 HCl was then used to treat CRC cells and assessed its effects on cell phenotypes in CRC cells with NUBP2 overexpression. Similar to NUBP2 deletion, GSK3 inhibitor CHIR-99021 HCl (10uM) inhibited proliferation and promoted apoptosis (Fig. 5B, C). On contrary, overexpression of NUBP2 had the opposite effects (Fig. 5B, C). Surprisingly, the pro-oncogenic effects of NUBP2 were significantly weakened by CHIR-99021 HCl. Collectively, these findings underscored the pivotal role of NUBP2 in regulating GSK-3, thereby influencing the phenotype of CRC cells.

Previous studies have demonstrated that the PI3K/AKT/GSK3β signaling pathway is implicated in the EMT and progression of CRC [17, 18]. Our investigation also demonstrated that knocking down NUBP2 effectively inhibited EMT in CRC (Fig. 3F). Furthermore, western blot analysis revealed an increase in the levels of phosphorylated GSK-3β,

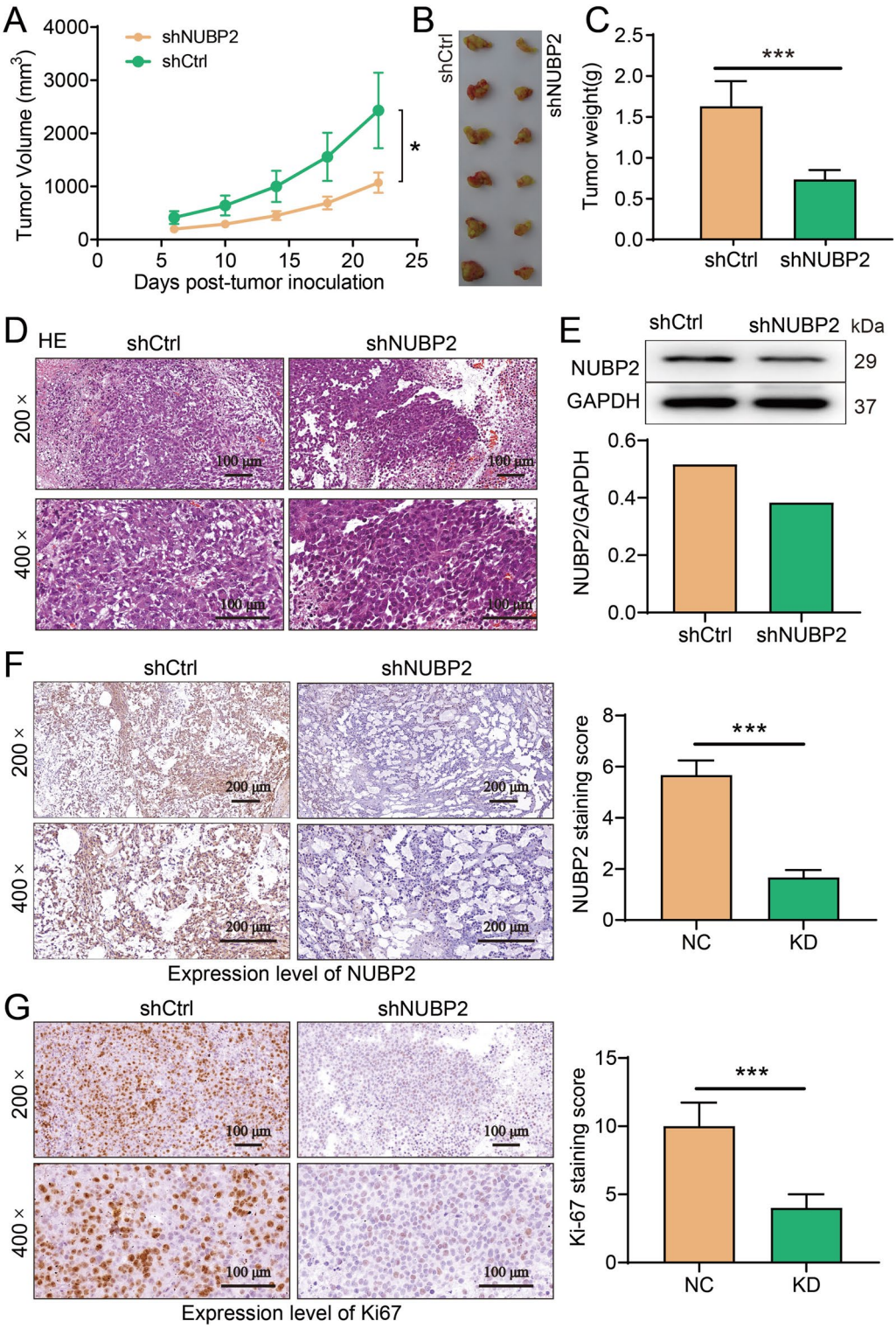

Fig. 4 Silencing of NUBP2 suppressed CRC xenograft tumor growth in mice. **A** The tumor volume was calculated to determine the tumor growth rates. **B** Tumor size was monitored with calipers. **C** Tumor weight of mice in the shCtrl group and shNUBP2 group was measured. **D** The tumor tissues from nude mice were subjected to HE staining. **E** NUBP2 protein levels in tumor tissues of mice between the two groups were measured by western blot analysis. **F** IHC staining of NUBP2 in mice tumor tissue. **G** Ki67 staining of tumor tissue were performed to assess cell proliferation in vivo. Results are presented as means ± SD. $^{*}P < 0.05$ and $^{***}P < 0.001$

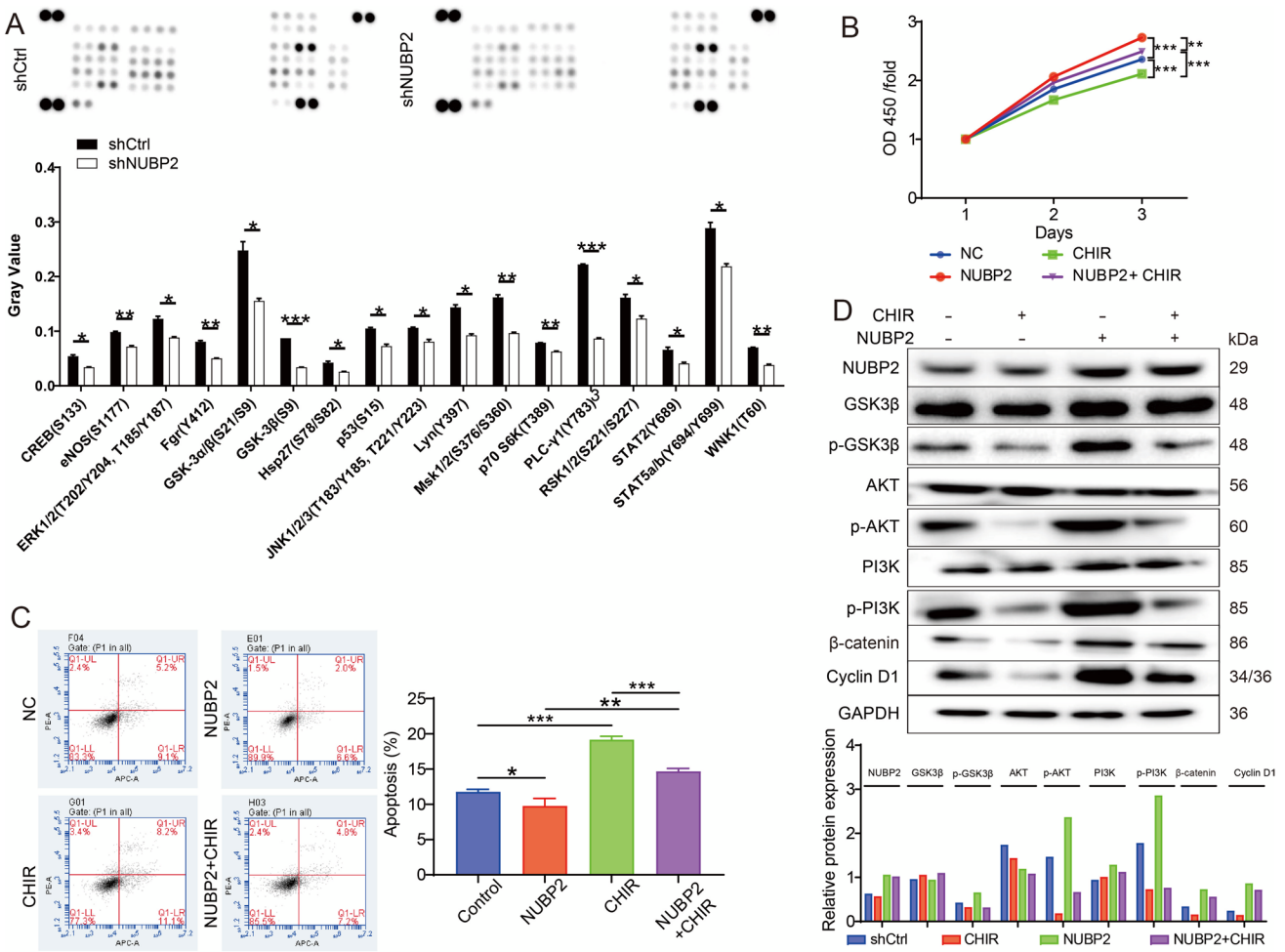

Fig. 5 NUBP2 exert critical roles in CRC progression via regulation of GSK-3β. **A** A human phospho-kinase array was performed in RKO cells upon NUBP2 knockdown. **B** CCK8 assay was performed to assess the proliferation of RKO cells with NUBP2 overexpression or CHIR-99021HCl (a GSK3 inhibitor) treatment. **C** The effect of NUBP2 overexpression on RKO cells apoptosis was assessed by flow cytometry in the presence or absence of CHIR-99021HCl. **D** The expression of NUBP2, GSK-3β, AKT, PI3K, β-catenin and Cyclin D1 was analyzed by western blot in RKO cells with NUBP2 overexpression and CHIR-99021HCl treatment. Results are presented as means ± SD. $^{*}P < 0.05$, $^{**}P < 0.01$ and $^{***}P < 0.001$

AKT and PI3K, as well as the protein levels of β-catenin, Cyclin D1 in RKO cells overexpressing NUBP2, which was partially reversed upon treatment with GSK3 inhibitor CHIR-99021 HCl (Figs. 5D and S1), implying that NUBP2 might regulate CRC EMT through PI3K/AKT/GSK3β signaling.

Discussion

CRC is a common malignant tumor, characterized by high incidence rate, metastasis rates and mortality, as well as poor prognosis [19]. Recently, a considerable body of evidence has implicated that identification of key molecular biomarker could improve molecular diagnosis and treatment of patients with CRC patients. Morever, NUBP2 has been found to disturb Fe–S cluster biogenesis and is responsible for regulating centrosome duplication and ribosome biogenesis in yeast [20]. Here, higher expression of NUBP2 was observed in CRC tissues and cell lines compared to para-carcinoma tissues and normal cells, and this elevated expression was associated with increased tumor malignancy. Therefore, this work focused on exploring the role NUBP2 plays in CRC.

NUBP2, a member of nucleotide-binding proteins (NUBP) [21], is involved in various physiological functions. Together with NUBP1, NUBP2 plays a critical role in the maturation of cytosolic and nuclear Fe–S proteins [22]. It has been discovered that the production of long splicing isoform of NUBP2 suppressed cancer cell proliferation in oral squamous cell carcinoma [23]. On the other hand, NUBP2 is required for cytosolic Fe/S protein assembly and cellular iron metabolism,

and its knockdown leads to reduced cell viability [24]. Consistently, our results demonstrated that NUBP2 knockdown resulted in suppressed cell proliferation and enhanced cell apoptosis in CRC cells. Whereas overexpressing NUBP2 promoted cell proliferation and suppressed apoptosis. Correspondingly, animal xenografts demonstrated that loss of NUBP2 resulted in a decreased tumor growth in vivo. The EMT is a biological process that contributes to the acquisition of mesenchymal cell features, and it has been demonstrated to increase invasiveness and migratory capabilities of CRC cells [25, 26]. Notably, the current study revealed that depleting NUBP2 effectively inhibited cell migration and invasion. This was confirmed by suppressing EMT through reducing N-cadherin and Vimentin expression, and increasing E-cadherin expression. These findings collectively indicated that NUBP2 plays a crucial role in promoting cancer development in CRC. Next, we attempted to preliminarily unveil the potential molecular mechanism by which NUBP2 regulated CRC progression.

Glycogen synthase kinase 3 beta (GSK3β) plays a crucial role in various biological processes such as cellular metabolism, cytoskeleton, and gene expression [27]. Moreover, GSK3β has been found to affect cell phenotypes like cell cycle, survival, proliferation, and apoptosis [28]. Previous studies have shown that GSK3β is upregulated or activated in CRC [29, 30]. Herein, we observed that the phosphorylation level of GSK-3β was suppressed in RKO cells when NUBP2 was knocked down, while upregulated upon NUBP2 overexpression. Notably, inhibiting GSK-3β led to cell cycle arrest and apoptosis in CRC [30]. Consistent with these findings, our findings demonstrated that treatment with CHIR-99021 HCl (10 μM), a GSK3 inhibitor, suppressed cell proliferation and facilitated apoptosis in CRC cells. What is more, the promoting effect of NUBP2 on the malignant behaviors of CRC cells could be reversed by the addition of CHIR-99021 HCl. Importantly, PI3K/AKT/GSK3β signaling pathway has been implicated in the EMT in CRC [17, 18]. Our study revealed that knocking down NUBP2 effectively inhibited EMT in CRC, while NUBP2 overexpression increased the expression of p-GSK-3β, p-AKT, p-PI3K, β-catenin and Cyclin D1. Interestingly, treatment with a GSK3 inhibitor partially reversed these effects, indicating that NUBP2 contributed to EMT and progression in CRC via GSK-3 regulation. However, further investigations are necessary to elucidate the precise mechanisms by which NUBP2 modulates EMT in CRC cells via the PI3K/AKT/GSK3β pathway.

Conclusion

In conclusion, our findings revealed that NUBP2 knockdown repressed malignant phenotype of CRC cells by suppressing cellular proliferation and migration while stimulating apoptosis, and inhibited tumor growth in vivo. Furthermore, restoring GSK3β activity could reverse the malignant phenotype of CRC cells induced by NUBP2 overexpression. Overall, the current study emphasized the potential of NUBP2 as a novel therapeutic target for combating CRC progression, providing valuable insights into the underlying mechanisms of CRC progression.

Supplementary Information The online version contains supplementary material available at https://doi.org/10.1007/s11010-024-04956-8.

Author contributions Bian Wu designed the project. Danfeng Lan, Junyu Wang, Guishun Sun and Yibo Wang performed the experiments. Danfeng Lan, Junyu Wang, Lixia Jiang, Qiyun Chen, Sha Li and Haiyan Qu performed data analysis. Danfeng Lan wrote the manuscript, and which passed all authors' check.

Funding This work was supported by the Yunnan health training project of high level talents (Grant Number: H-2019036), and the Yunnan Provincial Department of Science and Technology -Kunming Medical University Joint Special Project on Applied Basic Research (Grant Number: 202301AY070001-058).

Data availability The data set supporting the results of this article are included within the article.

Declarations

Competing interests The authors declare no competing interests.

Ethical approval This study was approved by Laboratory Animal Center, Kunming University of Science and Technology (No. KHLL2022-2778).

References

1. Weitz J, Koch M, Debus J, Höhler T, Galle P, Büchler M (2005) Colorectal cancer. Lancet (London, Engl) 365:153–165. https://doi.org/10.1016/s0140-6736(05)17706-x
2. Kang YH, Lee JS, Lee NH, Kim SH, Seo CS, Son CG (2021) Coptidis rhizoma extract reverses 5-fluorouracil resistance in HCT116 human colorectal cancer cells via modulation of thymidylate synthase. Molecules. https://doi.org/10.3390/molecules26071856
3. Ge Y, Xiang R, Ren J, Song W, Lu W, Fu T (2021) A nomogram for predicting multiple metastases in metastatic colorectal cancer patients: a large population-based study. Front Oncol 11:633995. https://doi.org/10.3389/fonc.2021.633995

4. Chen C, Xu ZQ, Zong YP, Ou BC, Shen XH, Feng H, Zheng MH, Zhao JK, Lu AG (2019) CXCL5 induces tumor angiogenesis via enhancing the expression of FOXD1 mediated by the AKT/NF-κB pathway in colorectal cancer. Cell Death Dis 10:178. https://doi.org/10.1038/s41419-019-1431-6
5. Piawah S, Venook A (2019) Targeted therapy for colorectal cancer metastases: a review of current methods of molecularly targeted therapy and the use of tumor biomarkers in the treatment of metastatic colorectal cancer. Cancer 125:4139–4147. https://doi.org/10.1002/cncr.32163
6. Biller L, Schrag D (2021) Diagnosis and treatment of metastatic colorectal cancer: a review. JAMA 325:669–685. https://doi.org/10.1001/jama.2021.0106
7. Chen Y, Bai B, Ying K, Pan H, Xie B (2022) Anti-PD-1 combined with targeted therapy: theory and practice in gastric and colorectal cancer. Biochim Biophys Acta 1877:188775. https://doi.org/10.1016/j.bbcan.2022.188775
8. Kypri E, Christodoulou A, Maimaris G, Lethan M, Markaki M, Lysandrou C, Lederer C, Tavernarakis N, Geimer S, Pedersen L, Santama N (2014) The nucleotide-binding proteins Nubp1 and Nubp2 are negative regulators of ciliogenesis. Cell Mol Life Sci (CMLS) 71:517–538. https://doi.org/10.1007/s00018-013-1401-6
9. Christodoulou A, Lederer C, Surrey T, Vernos I, Santama N (2006) Motor protein KIFC5A interacts with Nubp1 and Nubp2, and is implicated in the regulation of centrosome duplication. J Cell Sci 119:2035–2047. https://doi.org/10.1242/jcs.02922
10. Hinton TV, Batelu S, Gleason N, Stemmler TL (2022) Molecular characteristics of proteins within the mitochondrial Fe–S cluster assembly complex. Micron 153:103181. https://doi.org/10.1016/j.micron.2021.103181
11. DiStasio A, Paulding D, Chaturvedi P, Stottmann R (2020) Nubp2 is required for cranial neural crest survival in the mouse. Dev Biol 458:189–199. https://doi.org/10.1016/j.ydbio.2019.10.039
12. Phipps S, Garry C, Kamal S, Johnson J, Gilmer J, Long A, Kelleher D, Duggan S (2020) High content imaging of Barrett's-associated high-grade dysplasia cells after siRNA library screening reveals acid-responsive regulators of cellular transitions. Cell Mol Gastroenterol Hepatol 10:601–622. https://doi.org/10.1016/j.jcmgh.2020.05.002
13. Furutani M, Suganuma M, Akiyama S, Mitsumori R, Takemura M, Matsui Y, Satake S, Nakano Y, Niida S, Ozaki K, Hosoyama T, Shigemizu D (2023) RNA-sequencing analysis identification of potential biomarkers for diagnosis of sarcopenia. J Gerontol A Biol Sci Med Sci. https://doi.org/10.1093/gerona/glad150
14. Cai L, Sun Y, Wang K, Guan W, Yue J, Li J, Wang R, Wang L (2020) The better survival of MSI subtype is associated with the oxidative stress related pathways in gastric cancer. Front Oncol 10:1269. https://doi.org/10.3389/fonc.2020.01269
15. Zhao X, Chen J, Yin S, Shi J, Zheng M, He C, Meng H, Han Y, Han J, Guo J, Yuan Z, Wang Y (2022) The expression of cuproptosis-related genes in hepatocellular carcinoma and their relationships with prognosis. Front Oncol 12:992468. https://doi.org/10.3389/fonc.2022.992468
16. Li S, Liu Q, Wu D, He T, Yuan J, Qiu H, Tickner J, Zheng SG, Li X, Xu J, Rong L (2020) PKC-δ deficiency in B cells displays osteopenia accompanied with upregulation of RANKL expression and osteoclast-osteoblast uncoupling. Cell Death Dis 11:762. https://doi.org/10.1038/s41419-020-02947-3
17. Yao M, Li R, Yang Z, Ding Y, Zhang W, Li W, Liu M, Zhao C, Wang Y, Tang H, Wang J, Wen A (2020) PP9, a steroidal saponin, induces G2/M arrest and apoptosis in human colorectal cancer cells by inhibiting the PI3K/Akt/GSK3β pathway. Chem Biol Interact 331:109246. https://doi.org/10.1016/j.cbi.2020.109246
18. Long S, Wang J, Weng F, Xiang D, Sun G (2022) Extracellular matrix protein 1 regulates colorectal cancer cell proliferative, migratory, invasive and epithelial-mesenchymal transition activities through the PI3K/AKT/GSK3β/snail signaling axis. Front Oncol 12:889159. https://doi.org/10.3389/fonc.2022.889159
19. Sun Q, Xu K, Teng S, Wang W, Zhang W, Li X, Hu Z (2022) Construction of nomogram-based prediction model for clinical prognosis of patients with stage II and III colon cancer who underwent Xelox chemotherapy after laparoscopic radical resection. J Oncol 2022:7742035. https://doi.org/10.1155/2022/7742035
20. Okuno T, Yamabayashi H, Kogure K (2010) Comparison of intracellular localization of Nubp1 and Nubp2 using GFP fusion proteins. Mol Biol Rep 37:1165–1168. https://doi.org/10.1007/s11033-009-9477-7
21. Nakashima H, Grahovac M, Mazzarella R, Fujiwara H, Kitchen J, Threat T, Ko M (1999) Two novel mouse genes—Nubp2, mapped to the t-complex on chromosome 17, and Nubp1, mapped to chromosome 16—establish a new gene family of nucleotide-binding proteins in eukaryotes. Genomics 60:152–160. https://doi.org/10.1006/geno.1999.5898
22. Stehling O, Jeoung J, Freibert S, Paul V, Bänfer S, Niggemeyer B, Rösser R, Dobbek H, Lill R (2018) Function and crystal structure of the dimeric P-loop ATPase CFD1 coordinating an exposed [4Fe–4S] cluster for transfer to apoproteins. Proc Natl Acad Sci USA 115:E9085–E9094. https://doi.org/10.1073/pnas.1807762115
23. Ji M, Lv Y, Chen C, Xing D, Zhou C, Zhao J, Qi Y, Zhang J, Wang Y, Ma X, Xu W, Zhang W, Li X (2023) Metformin inhibits oral squamous cell carcinoma progression through regulating RNA alternative splicing. Life Sci 315:121274. https://doi.org/10.1016/j.lfs.2022.121274
24. Johnson N, Deck K, Nizzi C, Eisenstein R (2017) A synergistic role of IRP1 and FBXL5 proteins in coordinating iron metabolism during cell proliferation. J Biol Chem 292:15976–15989. https://doi.org/10.1074/jbc.M117.785741
25. Yang C, Dou R, Wei C, Liu K, Shi D, Zhang C, Liu Q, Wang S, Xiong B (2021) Tumor-derived exosomal microRNA-106b-5p activates EMT-cancer cell and M2-subtype TAM interaction to facilitate CRC metastasis. Mol Ther 29:2088–2107. https://doi.org/10.1016/j.ymthe.2021.02.006
26. Hu X, Xing W, Zhao R, Tan Y, Wu X, Ao L, Li Z, Yao M, Yuan M, Guo W, Li S, Yu J, Ao X, Xu X (2020) HDAC2 inhibits EMT-mediated cancer metastasis by downregulating the long noncoding RNA H19 in colorectal cancer. J Exp Clin Cancer Res 39:270. https://doi.org/10.1186/s13046-020-01783-9
27. Bolidong D, Domoto T, Uehara M, Sabit H, Okumura T, Endo Y, Nakada M, Ninomiya I, Miyashita T, Wong RW, Minamoto T (2020) Potential therapeutic effect of targeting glycogen synthase kinase 3β in esophageal squamous cell carcinoma. Sci Rep 10:11807. https://doi.org/10.1038/s41598-020-68713-9
28. Heng D, Wang Q, Ma X, Tian Y, Xu K, Weng X, Hu X, Liu W, Zhang C (2019) Role of OCT4 in the regulation of FSH-induced granulosa cells growth in female mice. Front Endocrinol (Lausanne) 10:915. https://doi.org/10.3389/fendo.2019.00915
29. Mishra R (2010) Glycogen synthase kinase 3 beta: can it be a target for oral cancer. Mol Cancer 9:144. https://doi.org/10.1186/1476-4598-9-144
30. Shakoori A, Mai W, Miyashita K, Yasumoto K, Takahashi Y, Ooi A, Kawakami K, Minamoto T (2007) Inhibition of GSK-3 beta activity attenuates proliferation of human colon cancer cells in rodents. Cancer Sci 98:1388–1393. https://doi.org/10.1111/j.1349-7006.2007.00545.x